Appl. Phys. A 90, 389–394 (2008)
DOI: 10.1007/s00339-007-4330-0

Applied Physics A
Materials Science & Processing

GEUN HYUNG KIM✉
HYEON YOON

A direct-electrospinning process by combined electric field and air-blowing system for nanofibrous wound-dressings

Bio-Mechatronics Team, Division of Nano Mechanical System, Korea Institute of Machinery and Materials, 171 Jang-dong, Yuseong-gu, Daejeon 305-343, Korea

Received: 24 September 2007/Accepted: 15 October 2007
Published online: 15 November 2007 •

ABSTRACT An electrospinning process has been introduced to fabricate micro/nanofiber membranes having high porosity and specific surface area. When constantly/uniformly depositing the micro/nanofiber membrane on a target, the electrospun fibers require flushing out of the high charge and excessive remaining solvent built up, since these factors can interrupt the constant deposition rate of the electrospun fibers on substrates. These limitations can be overcome with a direct-electrospinning process, which can lower the charges of the electrospun fibers through a window of guiding electrodes and remaining solvent of the electrospun fibers during the spinning process by an air-blowing system. Because of the reduced charge accumulation of the electrospun fibers, the micro/nanofibers can be deposited on any kind of target, which may be a conductive or a non-conductive material. The fabricated membrane had a dramatically reduced charge, remaining solvent concentration, sufficient tensile modulus, and small pore-size distribution. To observe the possibility as a biomedical wound-dressing material, a bacteria-shielding test of the fabricated membrane was conducted.

PACS 47.65.-d; 81.16.-c; 81.07.-b; 61.41.+e; 87.85.J-

1 Introduction

A variety of synthetic materials have been used as wound dressings to deal with the wide variety of wounds and many stages of healing, including hydrogels, chitosan, alginates, polyurethane or silicone foams, poly(ε-caprolactone) (PCL), and collagen [1–5]. To be effective, all of these wound-dressing materials must maintain a moist environment at the wound/dressing interface, provide mechanical protection, prevent bacterial penetration, allow gas–fluid exchange, be non-adherent to the wound and easily removed without trauma, and be non-toxic [6–10]. It was proposed that to fabricate a wound-covering membrane for use as a wound dressing, the membrane should have pore sizes ranging over 500–1000 nm to prevent bacterial penetration, and have a high surface area ranging over 5–100 m^2/g to promote proper fluid management and allow dermal delivery [11].

✉ Fax: +82-42-868-7933, E-mail: gkim@kimm.re.kr

Polymer nanofibers have recently been introduced as a wound-dressing material for treating wounds or burns of human skin because of their efficient gas–fluid exchange, controlled degraded formation, and reliable protection from bacterial penetration [3, 4, 11, 12]. Generally, the nanofibers have been fabricated using various electrospinning processes, including specially designed collectors, a microelectromechanical system (MEMS) nozzle tip, and an auxiliary electrode stabilizing initial spun jets [11, 13–18]. Fabricated electrospun fibers have also been used for a variety of applications, such as filter media, nano/biosensors, military protective coatings, three-dimensional scaffolds, composites, and drug delivery [11, 18–25].

As stated by other researchers, the electrospun membrane kept exudate fluid from the wound area and inhibited the invasion of exogenous micro-organisms because of the fine pores [3, 26]. In addition, electrospun nanofiber membranes have been used to deliver antibiotics to treat wounds [4, 19]. There is a particular advantage to this system because of the possibility of delivering uniform, highly controlled doses of bioactive agents at the wound area by taking advantage of the high surface-to-volume ratio of the nanofiber system [4]. However, although electrospun fibers have been recommended as wound dressings or protective coating materials, there are still limitations that need addressing. For example, there is insufficient control of residual charge density and remaining solvent within electrospun nanofibers when depositing the micro/nanofiber membrane. These factors can interrupt the constant deposition rate of electrospun fibers on a substrate. Moreover, these can influence the pore-size distribution and mechanical properties of the membrane, and eventually affect the wound-healing rate and the efficiency of the protective filtering system.

In this paper, we describe a directly fabricated membrane deposited on a substrate using a newly designed direct-electrospinning system (Fig. 1). In this system, the electrospun micro/nanofibers can be deposited on a substrate directly through an ac field controllable guiding electrode used to eliminate static charges in the electrospun fibers and an air-blowing system which was applied only in the whipping zone of the electrospun fibers, while standard electrospinning methods have shortcomings when it comes to obtaining deposition on a substrate because the spun fibers are highly charged and scattered over too wide an area, due

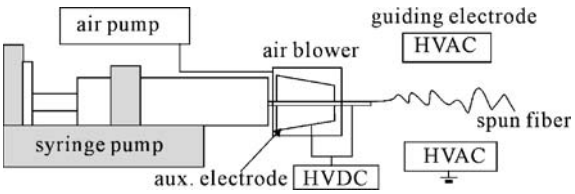

FIGURE 1 Schematic of the wound dresser using an electrospinning process that includes supporting electrodes (a conical electrode and guiding electrodes) and an air-streaming system

to the charged fibers and remaining solvent within the fibers. Using this method, we obtained a tailor-made membrane of micro/nanofibers with a high charge reduction and dramatically reduced remaining solvent compared to a normal electrospinning process.

2 Experimental

A polymer solution was prepared by dissolving 2.4 g of poly(ε-caprolactone) (PCL) in 30 g of a solvent mixture consisting of methylene chloride (MC; Junsei Chemical) and *N*, *N*-dimethyl formamide (DMF; Junsei Chemical) in a MC/DMF wt.% concentration. The PCL (M_n = 80 000; Sigma-Aldrich) was a semi-crystalline polymer used as a biomaterial because of its favorable mechanical properties and low melting point (around 55 °C); in addition, PCL is biodegradable and bioresorbable. The electrical conductivity, surface tension, and viscosity of the PCL solution used for the electrospinning process were 1.71 μS/cm, 36 mN/m, and 219 cP, respectively.

The electrospinning setup consisted of a conical electrode (the inner diameter near the nozzle was 25 mm) to support stable initial spin jets, guiding electrodes to provide stable spraying of the electrospun fibers on the substrate, and an air-blowing system to accelerate evaporation of the solvent. The applied range of ac electric field of the guiding electrode was 0.3–1 kV/cm to make the spun fibers converge between the electrodes.

The polymer solution was placed in a 20 mL glass syringe with a 20-gauge needle. The flow rate of the polymer solution was controlled using a syringe pump system (KDS 230; NanoNc). A high-voltage dc electric field was generated using a high-voltage amplifier (SHV300RD-50K; Convertech) at the nozzle tip and a conical electrode. The guiding electrodes were fabricated from a thin copper film and subjected to a high-voltage ac electric field that was generated using a high-voltage amplifier (610E; Trek) and a function generator (AFG310; Tektronix). Filtered air was controlled with the air controller using air pressures of 0.02 and 0.04 MPa.

The influence of the auxiliary electrode on this process is evident in photographs taken with a high-speed camera (FASTCAM Ultima APX RS; Photron).

The morphology of the electrospun fiber membrane was observed under an optical microscope (BX FM-32; Olympus) connected to a digital camera, and under a scanning electron microscope (SEM; Sirion).

To observe the effect of air blowing on the solvent in the electrospun membrane, a square ($5 \times 5\,\mathrm{cm}^2$) electrospun membrane was immediately transferred to a high-precision balance (BS224S; Sartorius) set in a chamber with constant humidity and temperature (45% and 26 °C), and the weight change with time was measured. The pore-diameter distribution and porosity of a PCL membrane (140 μm in thickness) fabricated using a guiding electrode and blowing air were measured using an AutoPore IV mercury porosimeter (Micromeritics Instruments, Norcross, GA). The reduced charge on the electrospun fibers was measured using a nanocoulomb meter (Monroe-284; Monroe) connected to a Faraday cup. The electrospun fiber membrane ($5 \times 7\,\mathrm{cm}^2$), which was deposited in 3 min on a poly(ethylene terephthalate) film (100-μm thick and $1 \times 10^5\ \Omega$ surface resistance), was immediately transferred to the Faraday cup. The mechanical behavior was characterized using a dynamic mechanical analyzer (DMA-Q800; TA Instruments) in tensile mode and a universal test machine (Nano UTM; MTS). Samples measuring $2 \times 12\,\mathrm{mm}^2$ were prepared, and their thicknesses were measured at five different points under an optical microscope and the measured values were averaged. To carry out the protection test from microorganisms, LB (Luria Bertani) plates were used. An LB plate is the most commonly used plate to grow bacteria such as *E. coli* because the plate is very efficient at stimulating growth. The electrosprayed nanofibers were deposited on an LB plate for the protection test. *E. coli* (SURE 2) was spread on a nanofiber membrane of the LB plates and the LB plates were incubated at 37 °C for 12 h. The bacteria were observed with the optical microscope.

3 Results and discussion

To attain a stable nanofiber membrane, the initial stability of the Taylor cone in the electrospinning system is extremely important. However, in a real system of an electrospinning process, the initial spun jet can easily go to an unstable state due to its processing and environmental conditions, such as near charged/scattered fibers, Fig. 2. To overcome these difficulties, an auxiliary conical electrode which was connected with a spinning nozzle and which can be charged

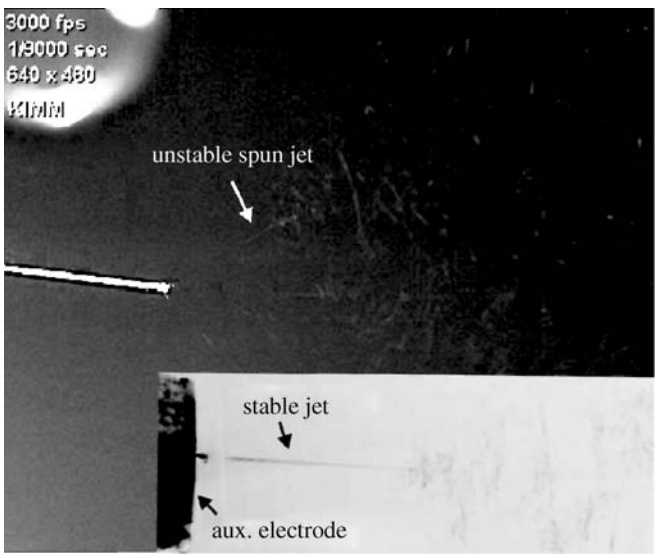

FIGURE 2 High-speed photographic images of initial spun jets showing the influence of an auxiliary electrode and a normal electrospinning process

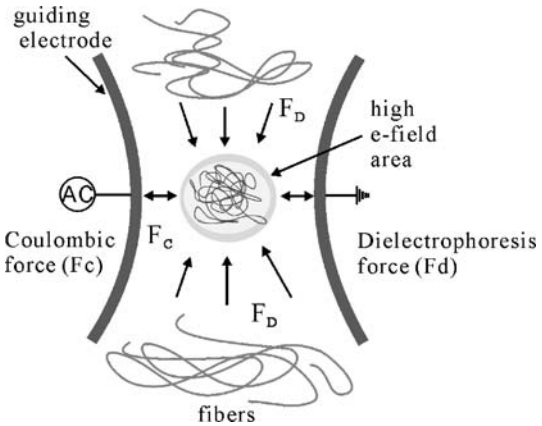

FIGURE 3 Schematic description of a simple mechanism of field-controllable guiding electrodes to concentrate the spun fibers in the electrospinning process

simultaneously as the liquid polymer passed through the spinneret was employed. As shown in the inset picture of Fig. 2, the auxiliary electrode served to reduce the instability of the initial jet leaving the apex of the Taylor cone and it provided a constant whipping motion of electrospun fibers. The detailed functions and computer-simulated results are described in Kim et al. [15].

Figure 3 shows the simple mechanism leading to the concentration of nano/microfibers between the guiding electrodes. The electrostatic movement of spun fibers in the ac field of the guiding electrodes may be considered to be subjected to a dielectrophoretic force (F_D) and a columbic attraction force (F_c). If randomly distributed nano/microfibers are in the air and under an externally applied electric field of the guiding electrodes, the fibers may interact electromechanically through the use of their induced dipole moment. The dielectrophoretic force of nanofibers can describe the physical phenomena resulting from the interaction between the induced polarization moment (μ) and the gradient of the applied electric field, and the dielectrophoretic force acting on a fiber in a non-uniform electric field, $\nabla E \neq 0$, can be expressed as $F_D = (\mu \cdot \nabla)E$, where μ $(= \varepsilon_0 \varepsilon_c \beta_F VE)$ is the dipole moment and E is the electric field [27]. The dipole moment is proportional to its volume, V, relative dielectric constant of the surrounding medium ε_c, and permittivity of free space $\varepsilon_0 = 8.8542 \times 10^{-12}$ F/m. A dimensionless parameter β_F is composed with the dielectric constant and the conductivity of the fiber and it is dependent on given shape, material, and applied electrical frequency [27, 28]. From this mechanism, to effectively concentrate the spun fibers, we have to maximize the parameter β_F, and the parameter is critically dependent on the frequency of the electric field. In the following paragraphs, we deal with the frequency effect on the electrospinning system.

The electrospinning stability of the electrospun fibers was highly dependent on the ac electric field placed on the guiding electrode. Figure 4 shows the effect of the applied frequency on the spinability of micro/nanofibers in this system. In Fig. 4a, the guiding electrode was grounded and a constant airflow of 0.04 MPa was applied to the nozzle tip. As expected, the electrospun nanofibers did not pass through the window between the guiding electrodes despite the steady airflow. In Fig. 4b, the guiding electrode was applied with the electric field (0.6 kV/cm and 0.1 Hz) and Fig. 4c was acquired under 0.6 kV/cm and 300 Hz. In both cases, the airflow pressure was 0.4 MPa. From the results, at the low-frequency range (roughly below 100 Hz) electrospun fibers did not go through the window of the parallel electrodes and connected between the parallel electrodes even though there was airflow. However, at the high-frequency region (over 300 Hz) the electrospun fibers were converged into the middle between the parallel electrodes and stably sprayed out to the environment. In addition, as shown in the magnified figure of Fig. 4c, the initial spun jets were incredibly stable. These results indicate that controlling the frequency applied to the guiding electrode can stabilize the initial straight jet of the process. The appropriate frequency range may be dependent on the electrical and rheological properties of the electrospun polymeric liquid, environmental conditions such as air temperature and humidity, and processing parameters, such as the flow rate and nozzle diameter. From these results, we are convinced that the role of the ac controllable guiding electrode can provide a path for the charged fibers to the desired substrates. In addition, using a stable, steady air-blowing system accelerated evaporation of the remaining solvent within the spun fibers and reduced the residual charges in the fiber mat. The detailed results are discussed in the next results of the charge-density measurement and remaining solvent within the spun fibers.

Figure 5a and b compare the dependence of the dc voltage applied on a nozzle tip and the distance from the guiding electrode to a substrate, respectively. An ac electric field (0.6 kV/cm and 300 Hz) of the guiding electrode and a constant airflow of 0.4 MPa were applied. As a well-known phenomenon, the applied voltage influenced the size distribution of the spun fibers. With a low voltage (16 kV), the electrospun fibers had diameters of 2.20 ± 1.1 μm while, with high voltage (24 kV), the distribution of the fiber diameters had a broad

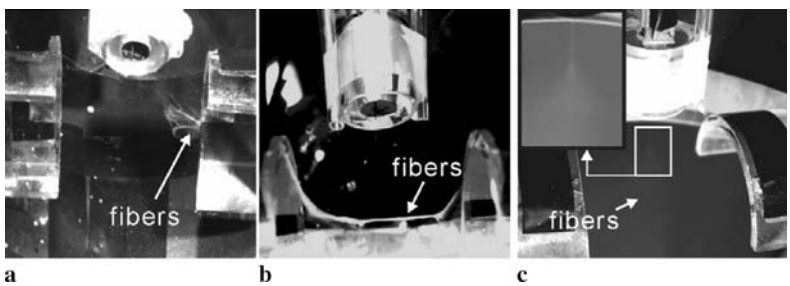

FIGURE 4 The photographs show the effect of applied frequency in the electrospraying process with the guiding electrodes and air-blowing system. (**a**) The electrospun fibers are shown attached to the guiding electrode. (**b**) The applied electric field was 18 kV at the nozzle and conical electrode and 0.6 kV/cm and 0.1 Hz at the parallel electrode with airflow of 0.4 MPa; (**c**) 18 kV at the nozzle and conical electrode and 0.6 kV/cm and 300 Hz at the parallel electrode with airflow of 0.4 MPa. Magnified picture in (**c**) shows a stable Taylor cone spraying from a nozzle

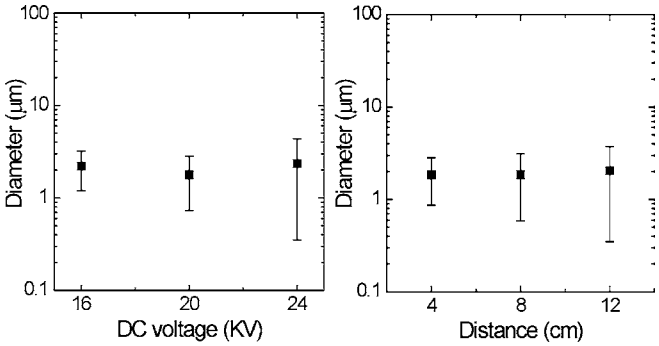

FIGURE 5 Dependence of the electrospun fiber diameter on (**a**) applied dc voltage on a nozzle tip and a conical electrode and (**b**) distance between the guiding electrode and the substrate

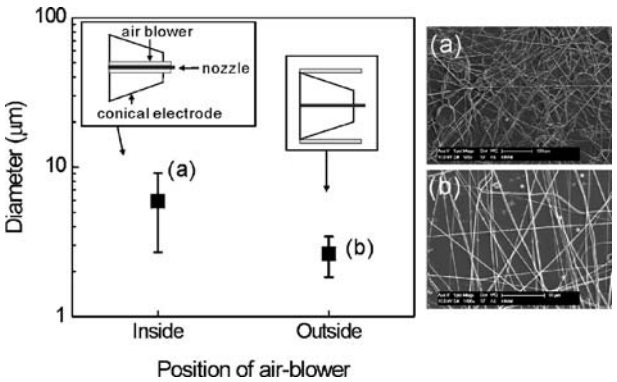

FIGURE 6 Dependence of the electrospun fiber diameter on the position of air-blowing system. The SEM images show micro/nanofibers electrospun on poly(ethylene terephthalate) film (**a**) with the air-blowing system set inside a conical electrode and (**b**) outside a conical electrode with a pressure of 0.04 MPa

range from 350 nm to 4.2 μm. On changing the distance from the edge of the guiding electrode to the target plate, the average diameter of the spun fibers was not changed, while the standard deviation of the diameter of the spun fibers was affected since the blown air accelerated the whipping motion of the spun fibers on increasing the distance between the guiding electrode and the target (see Fig. 5b).

The airflow system in the electrospinning process was firstly suggested by Chu and co-workers [29]. According to their results, a normal electrospinning process combined with an air-blowing system increased the solvent-evaporation rate and stabilized the formation of nanofibers, which varied with air-flow rate and blowing air temperature. In their setup, the air-blowing system was directly contacted with the nozzle tip of the Taylor cone. However, in our system, the direct contact with a nozzle tip and an air flow caused high instability of the Taylor cone and the spinability was poor. Figure 6 shows the effects of the position of the air-blowing system, inside the conical electrode (Fig. 6a) and outside the conical electrode (Fig. 6b), on the spinability of an electrospinning process. The nozzle and conical electrode were supplied with a dc voltage of 20 kV and an ac electric field of 0.6 kV/cm and 300 Hz with a constant airflow of 0.4 MPa. In this system, the direct contact with the nozzle tip of the Taylor cone and the blowing air caused unstable behavior in the initial spin jets, so that the diameter of spun fibers had a high value of standard deviation and a lot of beads were obtained, while stable initial spun jets

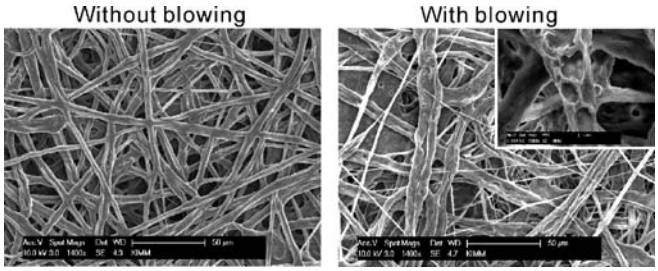

FIGURE 7 The SEM images show micro/nanofibers electrospun on poly(ethylene terephthalate) film without the air-blowing system and using the air-blowing system with a pressure of 0.04 MPa

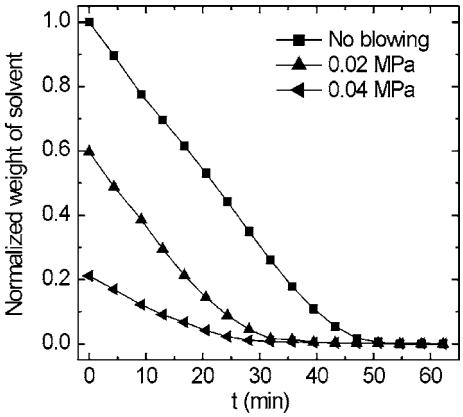

FIGURE 8 Normalized weight change of the solvent in electrospun membranes consisting of micro/nanofibers fabricated using the air-blowing system and guiding electrode

and a low value of standard deviation for the case using the air-blowing system setup outside the conical electrode (Fig. 6b) were achieved. Therefore, we used the air-blowing system setting outside the conical electrode. We believe that this stable electrospinability was due to the airflow just applied to the whipping zone of spun fibers. The surface morphology of the air-blown fibers also showed a high degree of roughness, as illustrated in Fig. 7. We believe that this phenomenon was due to the accelerated whipping behavior and fast evaporation of solvent caused by the air-blowing system.

Figure 8 shows the weight of electrospun membranes measured using a high-precision balance. PCL solution was electrospun onto a square ($5 \times 5\ \mathrm{cm}^2$) and transferred to the high-precision balance immediately. As shown in Fig. 8, the electrospun fibers still had remaining solvent within the stacked membrane but, when the air-blowing system was applied, the evaporation of solvent in the spinning process was accelerated and the remaining solvent was decreased dramatically. Roughly speaking, there was a 70% maximum reduction in remaining solvent using air blowing with a pressure of 0.04 MPa compared to not using air blowing. The remaining solvent in the membrane also decreased noticeably with time.

Figure 9 shows the reduced charges on the electrospun fibers, measured using a nanocoulomb meter connected to a Faraday cup. As the figure shows, the membrane's charges decreased dramatically with time and the trends of the charges on the fibers were consistent with each other. The charge reduction of the electrospun fibers through the ac field window was due to neutralization of the charges of the electrospun

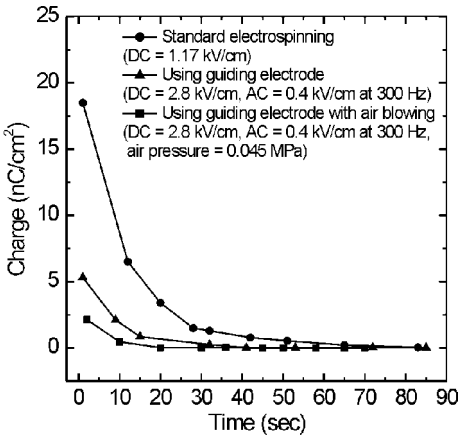

FIGURE 9 Plot of the surface charge density with time

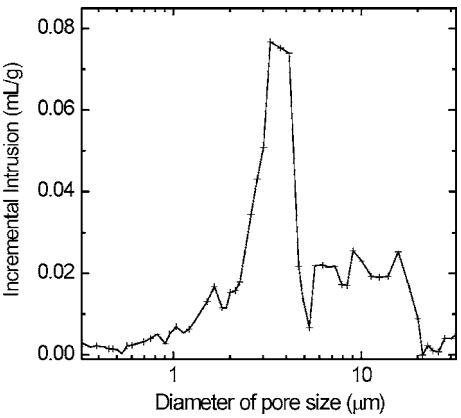

FIGURE 10 The distribution of pore-size diameter of the electrospun membrane

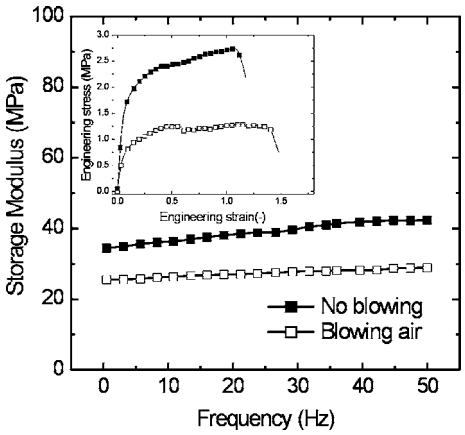

FIGURE 11 Storage modulus of the membrane and stress–strain curve

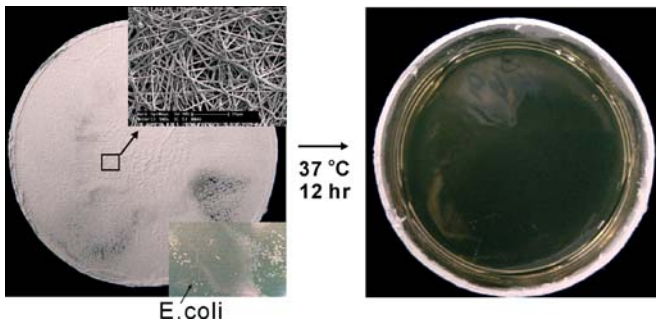

FIGURE 12 Protection test of nanofiber membrane sprayed on the LB plate from *E. coli* (SURE 2)

fibers. In addition, the charges of the fibers supplemented using the air-blowing system were reduced because the evaporation of solvent altered the concentration of the solution during the spinning process, which ultimately influences the diameter and charge density of the electrospun fibers [30, 31].

Pore size and pore-size distribution of the wound dressing or protective coating membrane are very important factors for preventing bacteria invasion and allowing gas and fluid exchange and dermal delivery. As shown in Fig. 10, there was a broad range of pore diameters from a few nanometers to hundreds of micrometers. The porosity of the fiber membrane was 70.3% and the average pore diameter was 53.4 nm. The total pore volume was 1.82 mL/g, and the total pore area was 136.5 m^2/g. We believe that a membrane with this pore-size distribution can protect a wound from various bacteria, and is amenable to fluid and dermal exchange.

The results in Fig. 11 were obtained using a dynamic mechanical analyzer in tensile mode (strain = 1.5%) at room temperature. In general, the mechanical properties of electrospun fiber mats depend strongly on the fiber orientation within the material, bonding between fibers due to the remaining solvent, and the slip of one fiber over another [32]. The storage moduli of the PCL membranes are shown in Fig. 11. For specimens fabricated using the air-blowing system, the membrane had an elastic modulus that was about 20% lower than membranes fabricated without an air-blowing system. This can be explained by the reduction in interconnecting adhesions between individual fibers caused by increasing the solvent-evaporation rate during the air-blowing process. According to Hollister, an adequate range of a mechanical modulus able to support excessive deformation in the scaffold of soft tissue is 0.4–350 MPa; hence, the tensile modulus (27 MPa) of the electrospun membrane as a wound-healing material should be sufficient [33]. The stress–strain curve for the electrospun membrane is seen in the inset in Fig. 11. According to the results, the Young's modulus of the membrane fabricated with and without air blowing was 19 and 33 MPa, respectively. This trend was similar to that obtained using the dynamic mechanical analyzer. In addition, the strain at the breaking point of the membrane was 1.41 and 1.09 with and without the air-blowing system. This implies that although the use of air blowing in the system may decrease the elastic modulus of the membrane, a membrane with an adequate modulus and high breaking strain can easily mould to human skin or any substrate. Previous results showed that use of the modified electrospinning process allows the electrospinning of micro/nanosized fibers onto living tissue.

To demonstrate the feasibility of this technique for a wound dresser, we carried out a protection test from microorganisms. As Fig. 12 shows, the micro/nanofibers were electrosprayed on an LB plate for the protection test, and the microorganism (*E. coli*) was spread on the electrosprayed fiber web using an air spray. After incubating on the electrospun membrane for 12 h at 37 °C, the membrane was removed from the LB plate. As shown in Fig. 12, a bacterial colony was not observed on the LB plate. This result showed a possibility as a membrane protecting the invasion of bacteria

and microorganisms. The average pore size and porosity of the membrane were about 53.4 nm and 70.27%, respectively. When compared with a bacterial pore size of 0.5–500 μm, the electrospun fiber membrane provided the protection ability as a cost-effective shielding material against bacteria.

4 Conclusions

In summary, we introduced a direct-electrospinning apparatus that uses a guiding electrode and an air-blowing system to enable the fabrication of wound-dressing membranes consisting of biodegradable PCL micro/nanofibers. Stable, steady deposition of electrospun fibers on any substrate occurred without interrupting the charges on the substrate. The membrane had a highly reduced charge and sufficient removal of solvent. Moreover, the membrane had a broad range of small pores, which should prevent bacteria invasion, and sufficient mechanical properties to sustain internally/externally applied mechanical stress.

ACKNOWLEDGEMENTS This work has been supported in part by a Basic Research Fund of the Korea Institute of Machinery and Materials (KIMM) on developing mechanical technology for biomaterials awarded to the Department of Future Technology.

REFERENCES

1 L.J. Hinrichs, E.J. Lommen, C.R.H. Widevuur, J. Feijen, J. Appl. Biomater. **2**, 287 (1992)
2 L.S. Leipziger, V. Glushko, B. DiBernado, F. Shafaie, J. Noble, J. Nichols, O.M. Alvarez, J. Am. Acad. Dermatol. **12**, 409 (1985)
3 M.S. Khil, D.I. Cha, H.Y. Kim, I.S. Kim, N. Bhattarai, J. Biomed. Mater. Res. Part B **67**, 675 (2003)
4 D.S. Katti, K.W. Robinson, F.K. Ko, C.T. Laurencin, J. Biomed. Mater. Res. Part B **70**, 286 (2004)
5 L. Wang, E. Khor, A. Wee, L.Y. Lim, J. Biomed. Mater. Res. Part B **63**, 610 (2002)
6 I.V. Yannas, J.F. Burke, J. Biomed. Mater. Res. **14**, 65 (1980)
7 I.V. Yannas, J.F. Burke, P.L. Gordon, J. Biomed. Mater. Res. **14**, 107 (1980)
8 N. Dagalakis, J. Flink, P. Stasikelis, J.F. Burke, I.V. Yannas, J. Biomed. Mater. Res. **14**, 511 (1980)
9 K. Matsida, S. Suzuki, N. Isshikin, K. Yoshioka, R. Wada, S.H. Hyun, Y. Ikada, Biomaterials **13**, 119 (1992)
10 M.C. Robson, B.D. Stenberg, J.D. Heggers, Clin. Plast. Surg. **3**, 485 (1990)
11 Z.M. Huang, Y.Z. Zhang, M. Kotaki, S. Ramakrishna, Compos. Sci. Technol. **63**, 2223 (2003)
12 E.-R. Kenawy, J.M. Layman, J.R. Watkins, G.L. Bowlin, J.A. Matthews, D.G. Simpson, G.E. Wnek, Biomaterials **24**, 907 (2003)
13 R. Dersch, M. Steinhart, U. Boudriot, A. Greiner, J.H. Wendorff, Polym. Adv. Technol. **16**, 276 (2005)
14 J. Kameoka, H.G. Craighead, Appl. Phys. Lett. **83**, 371 (2003)
15 G.H. Kim, H.S. Han, J.H. Park, W.D. Kim, Polym. Eng. Sci. **47**, 707 (2007)
16 W.E. Teo, S. Ramakrishuna, Nanotechnology **17**, R89 (2006)
17 D.H. Reneker, I. Chun, Nanotechnology **7**, 216 (1996)
18 G.H. Kim, W.D. Kim, Appl. Phys. Lett. **89**, 013 111 (2006)
19 Q. Qi, P. Hu, J. Xu, A. Wang, Biomacromolecules **7**, 2327 (2006)
20 W.J. Li, C.T. Laurencin, E.J. Caterson, R.S. Tuan, F.K. Ko, J. Biomed. Mater. Res. **60**, 613 (2002)
21 J. Huang, S. Virji, B.H. Weiller, R.B. Kaner, J. Am. Chem. Soc. **125**, 314 (2003)
22 D. Adam, Nature **411**, 236 (2001)
23 G.G. Chase, D.H. Reneker, C. Shin, AIChE J. **51**, 3109 (2005)
24 P. Gibson, H. Schreuder-Gibson, D. Rivin, Colloid Surf. A **187–188**, 469 (2001)
25 M.G. McKee, J.M. Layman, M.P. Cashion, T.E. Long, Science **311**, 353 (2006)
26 J. Venugopal, L.L. Ma, S. Ramakrishuna, Tissue Eng. **11**, 847 (2005)
27 L.D. Landau, E.M. Lifshitz, *Electrodynamics of Continuous Media* (Pergamon, New York, 1984)
28 G.H. Kim, Y.M. Shkel, J. Mater. Res. **19**, 1164 (2004)
29 I.C. Um, D. Fang, B.S. Hsiao, A. Okamoto, B. Chu, Biomacromolecules **5**, 1428 (2004)
30 V.E. Kalayci, P.K. Patra, Y.K. Kim, S.C. Ugbolue, Polymer **46**, 7191 (2005)
31 S.V. Fridrikh, J.H. Yu, M.P. Brenner, G.C. Rutledge, Phys. Rev. Lett. **90**, 144 502 (2003)
32 M. Wang, H.J. Jin, D.L. Kaplan, G.C. Rutledge, Macromolecules **37**, 6856 (2004)
33 S.J. Hollister, Nat. Mater. **4**, 518 (2005)